A Comprehensive study of the rational function model for photogrammetric processing

Article *in* Photogrammetric Engineering and Remote Sensing · December 2001

CITATIONS
317

READS
246

2 authors:

Chao Tao
Central South University
44 PUBLICATIONS **1,165** CITATIONS

SEE PROFILE

Yong Hu
PCI Geomatics
35 PUBLICATIONS **1,004** CITATIONS

SEE PROFILE

A Comprehensive Study of the Rational Function Model for Photogrammetric Processing

C. Vincent Tao and Yong Hu

Abstract

The rational function model (RFM) has gained considerable interest recently mainly due to the fact that Space Imaging Inc. (Thornton, Colorado) has adopted the RFM[1] as an alternative sensor model for image exploitation. The RFM has also been implemented in some digital photogrammetric systems to replace the physical sensor mode for photogrammetric processing. However, there have been few publications addressing the theoretical properties and practical aspects of the RFM until recently. In this paper a comprehensive study of the RFM is reported upon. Technical issues such as the solutions, feasibility, accuracy, numerical stability, and requirements for control information are addressed. Both the direct and iterative least-squares solutions to the RFM are derived, and the solutions under terrain-dependent and terrain-independent computation scenarios are discussed. Finally, evaluations of the numerous tests with different data sets are analyzed. The objective of this study is to provide readers with a comprehensive understanding of the issues pertaining to applications of the RFM.

Background

Physical versus Generalized Sensor Models

Sensor models are required to establish the functional relationship between the image space and the object space. They are of particular importance to stereo reconstruction and image ortho-rectification. Sensor models are typically classified into two categories: physical and generalized models. The choice of a sensor model depends primarily on the performance and accuracy required, and the camera and control information available (McGlone, 1996).

A physical sensor model represents the physical imaging process. The parameters involved describe the position and orientation of a sensor with respect to an object-space coordinate system. Physical models, such as the collinearity equations, are rigorous, very suitable for adjustment by analytical triangulation, and normally yield high modeling accuracy (a fraction of one pixel). In physical models, parameters are normally uncorrelated because each parameter has a physical significance. Further refinement is also possible by extending the model with the addition of calibration parameters to describe effects known or effects suspected to be present.

Although rigorous physical sensor models are more accurate, the development of generalized sensor models independent of sensor platforms and sensor types becomes attractive. In a generalized sensor model, the transformation between the image and the object space is represented as some general function without modeling the physical imaging process. The function can be of several different forms, such as polynomials or rational functions.

Replacement Sensor Models

Sensor models are used extensively in photogrammetric reduction (e.g., stereo reconstruction, ortho-rectification, DEM generation, feature editing, quality checking, etc.). Many of the above applications require real-time implementations. Therefore, use of the generalized sensor model to replace the physical sensor model for real-time photogrammetric processing is a natural choice provided that the accuracy degradation is negligible (Paderes *et al.*, 1989). A further advantage is that the photogrammetric processing software can be kept unchanged when dealing with different sensor data because the generalized sensor model is sensor independent. For new sensors, only the values of coefficients in the generalized sensor model need to be updated. The concept of the replacement sensor model is not new and has been implemented in some commercial photogrammetric systems (Madani, 1999; Dowman and Dolloff, 2000; Tao and Hu, 2001a).

The key to the use of a replacement sensor model is that the replacement sensor model must fit the physical sensor model very well. Normally, the unknown coefficients in the replacement sensor model are solved using a 3D object grid and the corresponding image grid. The parameters of a replacement sensor model are then solved for by fitting the model to the object grid and corresponding image grid.

There are three replacement sensor models that have been used (OGC, 1999): the grid interpolation model, the RFM, and the universal real-time model. In the grid interpolation model, a 3D grid in ground space is generated and the image coordinates for each grid point are computed using a physical sensor model. To find the image coordinates corresponding to specified

[1]The terms Rational Polynomial Camera (RPC) model and Image Geometry Model (IGM) are used by Space Imaging in its product line. They are the same as the RFM when used in this context.

Department of Geomatics Engineering, The University of Calgary, 2500 University Dr., NW, Calgary, Alberta T2N 1N4, Canada (yhu@ucalgary.ca).

C.V. Tao is presently with the Geospatial Information and Communication (Geo-ICT) Lab, Dept. of Earth and Atmospheric Science, York University, 4700 Keele Street, Toronto, Ontario M3J 1P3, Canada (ctao@ucalgary.ca).

Photogrammetric Engineering & Remote Sensing
Vol. 67, No. 12, December 2001, pp. 1347–1357.

0099-1112/01/6712–1347$3.00/0

ground coordinates, the surrounding grid points are found. Trilinear interpolation is then used between these eight points. The grid interpolation model does not produce adequate accuracy. The RFM uses ratios of polynomials to establish the relationship between the image coordinates and the object coordinates. The universal real-time model is in fact an extension to the RFM. It employs interpolation of high-order correction functions. Because the RFM is the most popular model in use, the emphasis in this study is placed on the investigation of the RFM.

Characteristics of the RFM

Mathematically, the disadvantage of using polynomials for approximation is their tendency for oscillation. This often causes error bounds in polynomial approximation to significantly exceed the average approximation error. The RFM has better interpolation properties. It is typically smoother and can spread the approximation error more evenly between exact fit points. The RFM has the added advantage of permitting efficient approximation of functions that have infinite discontinuities near, but outside, the interval of fitting, while a polynomial approximation is generally unacceptable in this situation (Burden and Faires, 1997).

The RFM is independent of sensors and platforms. It also has coordinate system flexibility. It can accommodate object coordinates in any system such as geocentric, geographic, or any map projection coordinate system (Paderes *et al.*, 1989).

The RFM resembles projective equations very well (Madani, 1999). With adequate control information, the RFM can achieve a very high fitting accuracy with sufficient speed to support real time implementations. This is the primary reason why the RFM has been used as a replacement sensor model.

Because there are no functional relationships between the parameters of the physical sensor model and those of the RFM, the physical parameters can hardly be recovered from the RFM and the sensor information can be kept confidential. In order to protect the undisclosed sensor information, some commercial satellite data vendors, such as Space Imaging Inc., only provide users with the RFM instead of the physical sensor models. As a result, without knowing the physical sensor models, users are still able to perform photogrammetric processing such as ortho-rectification, stereo reconstruction, and DEM generation at no discernible loss of accuracy (Grodecki, 2001).

Introduction

The RFM is already available within some digital photogrammetric software packages (Madani, 1988; Paderes *et al.*, 1989; Greve *et al.*, 1992; Toutin and Cheng, 2000; Yang, 2000). Except for some experimental results reported, the research on the various aspects of the RFM has not been published. For this reason, the University of Calgary initiated a research project in 1999, "A Comprehensive Study on the RFM for Photogrammetric Processing" (Tao and Hu, 2001a). This paper addresses the important practical issues pertaining to the use of the RFM.

The derivation of the iterative and direct least-squares solution to the RFM is described in the next section. The two computational scenarios, i.e., terrain-independent and terrain-dependent, are then discussed. For the terrain-dependent scenario, where the physical sensor model is not available, a robust bucketing technique is proposed and developed for automatic selection of evenly distributed control points in ground space. Finally, several tests using both aerial photograph and SPOT data sets are described, and evaluations, findings, and conclusions are given.

Solutions to the Rational Function Model

Basic Equations

In the rational function model, image pixel coordinates (r, c) are expressed as the ratios of polynomials of ground coordinates (X, Y, Z). In order to minimize the introduction of errors during the computations and improve the numerical stability of equations, the two image coordinates and three ground coordinates are each offset and scaled to fit the range from -1.0 to $+1.0$ (NIMA, 2000). For the ground-to-image transformation, the defined ratios of polynomials have the following form for each image section (OGC, 1999):

$$r_n = \frac{p1(X_n, Y_n, Z_n)}{p2(X_n, Y_n, Z_n)} \tag{1a}$$

$$c_n = \frac{p3(X_n, Y_n, Z_n)}{p4(X_n, Y_n, Z_n)} \tag{1b}$$

where r_n and c_n are the normalized row and column indices, respectively, of pixels in image space, and X_n, Y_n, and Z_n are the normalized coordinate values of object points in ground space. The normalization of the coordinates is computed using the following equations (OGC, 1999):

$$r_n = \frac{r - r_o}{r_s}, \quad c_n = \frac{c - c_o}{c_s}$$

$$X_n = \frac{X - X_o}{X_s}, \quad Y_n = \frac{Y - Y_o}{Y_s}, \quad Z_n = \frac{Z - Z_o}{Z_s} \tag{2}$$

where r_o and c_o are offset values for the two image coordinates, and r_s and c_s are scale values for the two image coordinates. Similarly, X_o, Y_o, *and* Z_o are offset values for the three ground coordinates, and X_s, Y_s, and Z_s are scale values for the three ground coordinates.

The maximum power of each ground coordinate is typically limited to 3; and the total power of all ground coordinates is also limited to 3. In such a case, each polynomial is of 20-term cubic form (the subscripts are omitted for convenience): i.e.,

$$\begin{aligned} p = \sum_{i=0}^{m1}\sum_{j=0}^{m2}\sum_{k=0}^{m3} a_{ijk} X^i Y^j Z^k &= a_0 + a_1 Z + a_2 Y + a_3 X \\ &+ a_4 ZY + a_5 ZX + a_6 YX + a_7 Z^2 + a_8 Y^2 + a_9 X^2 \\ &+ a_{10} ZYX + a_{11} Z^2 Y + a_{12} Z^2 X + a_{13} Y^2 Z + a_{14} Y^2 X \\ &+ a_{15} ZX^2 + a_{16} YX^2 + a_{17} Z^3 + a_{18} Y^3 + a_{19} X^3 \end{aligned} \tag{3}$$

where a_{ijk} are polynomial coefficients called **rational function coefficients (RFCs)**. The order of the terms is trivial and may differ in different literature.

The distortions caused by the optical projection can generally be represented by the ratios of first-order terms, while corrections such as Earth curvature, atmospheric refraction, lens distortion, etc., can be well approximated by the second-order terms. Some other unknown distortions with high-order components, such as camera vibration, can be modeled with the third-order terms.

The RFM is essentially a generic form of polynomials. When the denominator is equal to 1, Equations 1a and 1b become regular 3D polynomials. The RFM resembles the projective equations, such as the Direct Linear Transformation (represented as the ratios of two first-order polynomials). A comparative study of the RFM with other imaging geometric models is given in Tao and Hu (2000b).

Iterative and Direct Least-Squares Solutions

Two methods have been developed to solve for the RFM, direct and iterative least-squares solutions (Tao and Hu, 2000a). The derivation of these two solutions is given below.

First, we can rewrite Equations 1a and 1b as

$$r = \frac{(1\ Z\ Y\ X \cdots Y^3\ X^3) \cdot (a_0\ a_1 \cdots a_{19})^T}{(1\ Z\ Y\ X \cdots Y^3\ X^3) \cdot (1\ b_1 \cdots b_{19})^T} \tag{4a}$$

$$c = \frac{(1\ Z\ Y\ X \cdots Y^3\ X^3) \cdot (c_0\ c_1 \cdots c_{19})^T}{(1\ Z\ Y\ X \cdots Y^3\ X^3) \cdot (1\ d_1 \cdots d_{19})^T} \tag{4b}$$

The observation error equations can then be formed as

$$v_r = \left[\frac{1}{\mathbf{B}}\ \frac{Z}{\mathbf{B}}\ \frac{Y}{\mathbf{B}}\ \frac{X}{\mathbf{B}} \cdots \frac{Y^3}{\mathbf{B}}\ \frac{X^3}{\mathbf{B}}\ -\frac{rZ}{\mathbf{B}}\ -\frac{rY}{\mathbf{B}} \cdots -\frac{rY^3}{\mathbf{B}}\ -\frac{rX^3}{\mathbf{B}}\right] \cdot \mathbf{J} - \frac{r}{\mathbf{B}} \tag{5a}$$

$$v_c = \left[\frac{1}{\mathbf{D}}\ \frac{Z}{\mathbf{D}}\ \frac{Y}{\mathbf{D}}\ \frac{X}{\mathbf{D}} \cdots \frac{Y^3}{\mathbf{D}}\ \frac{X^3}{\mathbf{D}}\ -\frac{cZ}{\mathbf{D}}\ -\frac{cY}{\mathbf{D}} \cdots -\frac{cY^3}{\mathbf{D}}\ -\frac{cX^3}{\mathbf{D}}\right] \cdot \mathbf{K} - \frac{c}{\mathbf{D}} \tag{5b}$$

or

$$v_r' = \mathbf{B}v_r = [1\ Z\ Y\ X \cdots Y^3\ X^3\ -rZ\ -rY \cdots -rY^3\ -rX^3] \cdot \mathbf{J} - r \tag{6a}$$

$$v_c' = \mathbf{D}v_c = [1\ Z\ Y\ X \cdots Y^3\ X^3\ -cZ\ -cZ\ -cY \cdots -cY^3\ -cX^3] \cdot \mathbf{K} - c \tag{6b}$$

where

$$\mathbf{B} = (1\ Z\ Y\ X \cdots Y^3\ X^3) \cdot (1\ b_1 \cdots b_{19})^{\mathrm{T}}$$
$$\mathbf{J} = (a_0\ a_1 \cdots a_{19}\ b_1\ b_2 \cdots b_{19})^{\mathrm{T}}$$
$$\mathbf{D} = (1\ Z\ Y\ X \cdots Y^3\ X^3) \cdot (1\ d_1 \cdots d_{19})^{\mathrm{T}}$$
$$\mathbf{K} = (c_0\ c_1 \cdots c_{19}\ d_1\ d_2 \cdots d_{19})^{\mathrm{T}}$$

Given n, the number of ground control points (GCPs) and the corresponding image points, the matrix form of Equation 5a can be written as

$$\begin{bmatrix} v_{r1} \\ v_{r2} \\ \vdots \\ v_{rn} \end{bmatrix} = \begin{bmatrix} \frac{1}{\mathbf{B}_1} & 0 & \cdots & 0 \\ 0 & \frac{1}{\mathbf{B}_2} & 0 & \vdots \\ \vdots & 0 & \ddots & 0 \\ 0 & \cdots & 0 & \frac{1}{\mathbf{B}_n} \end{bmatrix} \cdot \begin{bmatrix} 1 & Z_1 & \cdots & X_1^3 & -r_1Z_1 & \cdots & -r_1X_1^3 \\ 1 & Z_2 & \cdots & X_2^3 & -r_2Z_2 & \cdots & -r_2X_2^3 \\ \vdots & \vdots & \ddots & \vdots & \vdots & \ddots & \vdots \\ 1 & Z_n & \cdots & X_n^3 & -r_nZ_n & \cdots & -r_nX_n^3 \end{bmatrix} \cdot \mathbf{J} - \begin{bmatrix} \frac{1}{\mathbf{B}_1} & 0 & \cdots & 0 \\ 0 & \frac{1}{\mathbf{B}_2} & 0 & \vdots \\ \vdots & 0 & \ddots & 0 \\ 0 & \cdots & 0 & \frac{1}{\mathbf{B}_n} \end{bmatrix} \cdot \begin{bmatrix} r_1 \\ r_2 \\ \vdots \\ r_n \end{bmatrix} \tag{7a}$$

or

$$\mathbf{V}_r = \mathbf{W}_r\mathbf{M}\mathbf{J} - \mathbf{W}_r\mathbf{R} \tag{7b}$$

where

$$\mathbf{M} = \begin{bmatrix} 1 & Z_1 & \cdots & X_1^3 & -r_1Z_1 & \cdots & -r_1X_1^3 \\ 1 & Z_2 & \cdots & X_2^3 & -r_2Z_2 & \cdots & -r_2X_2^3 \\ \vdots & \vdots & \ddots & \vdots & \vdots & \ddots & \vdots \\ 1 & Z_n & \cdots & X_n^3 & -r_nZ_n & \cdots & -r_nX_n^3 \end{bmatrix},$$

$$\mathbf{R} = \begin{bmatrix} r_1 \\ r_2 \\ \vdots \\ r_n \end{bmatrix}, \quad \mathbf{W}_r = \begin{bmatrix} \frac{1}{\mathbf{B}_1} & 0 & \cdots & 0 \\ 0 & \frac{1}{\mathbf{B}_2} & 0 & \vdots \\ \vdots & 0 & \ddots & 0 \\ 0 & \cdots & 0 & \frac{1}{\mathbf{B}_n} \end{bmatrix}$$

$\mathbf{W}_r$ can be considered as the weight matrix for the residuals on the left side of Equation 6a. Consequently, the obtained normal equation is

$$\mathbf{M}^{\mathrm{T}}\mathbf{W}_r^2\mathbf{M}\mathbf{J} - \mathbf{M}^{\mathrm{T}}\mathbf{W}_r^2\mathbf{R} = 0 \tag{8}$$

If $\mathbf{W}_r$ is set to be the identity matrix, the direct solution of RFCs can be represented as

$$\mathbf{J} = (\mathbf{M}^{\mathrm{T}}\mathbf{M})^{-1}\mathbf{M}^{\mathrm{T}}\mathbf{R}. \tag{9}$$

For the iterative solution, the initial values $\mathbf{J}^{(0)}$ of the coefficients are first solved for using the direction solution method, i.e., Equation 9. Then $\mathbf{W}_r^{(i)}$ and $\mathbf{J}^{(i)}$ are calculated by solving the normal Equation 8 iteratively until the absolute difference of the residuals between two consecutive iterations is below some threshold. A check for zero crossing in the denominator $\mathbf{B}$ is performed during the computation in order to protect the weight matrix from division by zero.

Comparing the direct solution, Equation 9, and the iterative solution, Equation 8, the latter is theoretically more rigorous because the weights have been accounted for in the solution. The weight matrix multiplication is introduced to form the new design matrix of the normal equations in the iterative solution. By making this simplification of weighting, the direct solution is obtained. Therefore, the computational burden of each iteration is close to the time needed for the direct solution.

The solution of column-wise Equation 5b is the same as that of row-wise Equation 5a, provided that the symbols r, $\mathbf{B}$, $\mathbf{J}$, a, b, $\mathbf{R}$, and $\mathbf{M}$ in Equations 5 through 8 are replaced by c, $\mathbf{D}$, $\mathbf{K}$, c, d, $\mathbf{C}$, and $\mathbf{N}$, respectively. The row-wise and column-wise equations, Equations 5a and 5b, can be adjusted together. The following error equations can be used:

$$\begin{bmatrix} \mathbf{V}_r \\ \hline \mathbf{V}_c \end{bmatrix} = \begin{bmatrix} \mathbf{W}_r & | & 0 \\ \hline 0 & | & \mathbf{W}_c \end{bmatrix} \cdot \begin{bmatrix} \mathbf{M} & | & 0 \\ \hline 0 & | & \mathbf{N} \end{bmatrix} \cdot \begin{bmatrix} \mathbf{J} \\ \hline \mathbf{K} \end{bmatrix} - \begin{bmatrix} \mathbf{W}_r & | & 0 \\ \hline 0 & | & \mathbf{W}_c \end{bmatrix} \cdot \begin{bmatrix} \mathbf{R} \\ \hline \mathbf{C} \end{bmatrix} \tag{10}$$

or

$$\mathbf{V} = \mathbf{W}\mathbf{T}\mathbf{I} - \mathbf{W}\mathbf{G}.$$

The normal equation is

$$\mathbf{T}^{\mathrm{T}}\mathbf{W}^2\mathbf{T}\mathbf{I} - \mathbf{T}^{\mathrm{T}}\mathbf{W}^2\mathbf{G} = 0. \tag{11}$$

Similarly, after solving for the the initial values $\mathbf{I}^{(0)}$ of the

coefficients by the direct solution, $\mathbf{W}^{(i)}$ and the iterative solution $\mathbf{I}^{(i)}$ can be computed by solving the normal Equation 11 iteratively.

The combined form (Equation 11) is used in our experiments, but the results computed using Equation 8 and Equation 11 have only a trivial difference.

Regularization of the Normal Equation

It has been found that the values of the denominators B_i and D_i ($i = 1, n$) vary widely when the control points are not evenly distributed. As a result, the design matrix $\mathbf{T}$ becomes ill conditioned and the matrix $\mathbf{T}^T\mathbf{W}^2\mathbf{T}$ in normal Equation 11 could become singular. It happens often when the high order (i.e., more than second-order) polynomials in the RFM are used. The negative impact of this is that the iterative solution cannot be converged.

In order to improve the condition number of the matrix $\mathbf{T}^T\mathbf{W}^2\mathbf{T}$, we applied the regularization technique in which a small multiplication of the identity matrix $\mathbf{E}$ is added. Because $\mathbf{T}^T\mathbf{W}^2\mathbf{T}$ is usually symmetric and positive semi-definite, the matrix $\mathbf{T}^T\mathbf{W}^2\mathbf{T} + h^2\mathbf{E}$ has its eigenvalues in $[h^2, h^2 + \|\mathbf{T}^T\mathbf{W}^2\mathbf{T}\|]$ and, hence, a condition number is not greater than $(h^2 + \|\mathbf{T}^T\mathbf{W}^2\mathbf{T}\|)/h^2$, which becomes small as h^2 increases. With this modification, the normal Equation 11 turns into a regularized one: i.e.,

$$(\mathbf{T}^T\mathbf{W}^2\mathbf{T} + h^2\mathbf{E})\mathbf{I} - \mathbf{T}^T\mathbf{W}^2\mathbf{G} = 0. \tag{12}$$

To obtain a smoother solution, the above equation is solved iteratively using the Tikhonov method (Neumaier, 1998): i.e.,

$$\begin{aligned} &\mathbf{I}_{(0)} = 0,\ \mathbf{W}_{(0)} = \mathbf{W}(\mathbf{I}_{(0)}) = \mathbf{E}, \\ &\mathbf{I}_{(s)} = \mathbf{I}_{(s-1)}(\mathbf{T}^T\mathbf{W}^2_{(s-1)}\mathbf{T} + h^2\,\mathbf{E})^{-1}\mathbf{T}^T\mathbf{W}^2_{(s-1)}\mathbf{v}_{(s-1)} \text{ for } s = 1, 2, \ldots \end{aligned} \tag{13}$$

where $\mathbf{W}_{(s)} = \mathbf{W}(\mathbf{I}_{(s)})$, $\mathbf{v}_{(s)} = \mathbf{G} - \mathbf{T}\mathbf{I}_{(s)}$.

Determination of the regularization parameter h is nontrivial. Typically, solutions are computed for a large number of different h values, and the best one is selected by suitable heuristics, e.g., the L-curve based method (Neumaier, 1998).

In order to determine the best value of h, different values of h were tried in Equation 12. An experimental result is shown in Figure 1, where the third-order RFM was used. In this experiment, 60 GCPs and their corresponding image points were used to solve for the RFCs, and 249 checking points (CKPs) in an image were employed for accuracy checking. Based on the tests, it was found that a reasonably good convergence could be reached in six iterations or less in most cases when h is in the range of 0.0002 to 0.004. The result is also not sensitive to the particular h value as long as h is within that range (see Figure 1). Therefore, $h = 0.001$ was chosen for the rest of the tests.

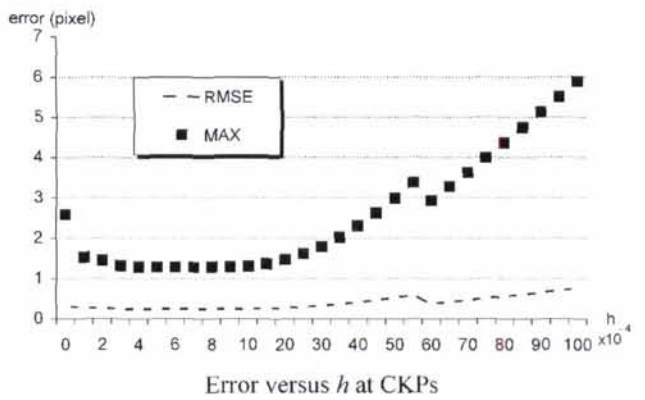

Error versus h at CKPs

Figure 1. Determination of regularization parameter h.

Terrain-Independent versus Dependent Computational Scenarios

The RFCs of the RFM can be solved for with or without knowing the physical sensor models. If the physical sensor model is available, the terrain-independent solution can be developed. Otherwise, the RFM solution will be highly dependent on the input control points from the terrain surface.

Terrain-Independent Computational Scenario

With the physical sensor model available, the RFM can be solved using an object grid with its grid-point coordinates determined using a physical sensor model. This method involves the following steps:

- *Determination of an Image Grid.* The image grid contains m by n image points. These points are evenly distributed across the full extent of the image. The number of rows m and columns n should be adequate (e.g., 10 by 10).
- *Establishment of a 3D Object Grid in Ground Space.* The physical sensor model is used to compute the point positions of the object grid (shown in Figure 2). The dimension of this 3D grid is based on the full extent of the image and the range of the estimated terrain relief, i.e., the dimension of the grid covers the range of the 3D terrain surface. The grid contains several elevation layers. To prevent the design matrix from becoming ill-conditioned, the number of layers should be greater than three (based on our experience).
- *RFM Fitting.* The unknown RFCs are then solved for using the corresponding image and object grid points.
- *Accuracy Checking.* A check object grid is generated in a similar way but with double density in each dimension. The obtained RFM is then used to calculate the image positions of the check object grid points. By calculating the difference between the coordinates of the original image grid points and those calculated from the RFM, the accuracy of the RFM can be evaluated.

The above method can be used to determine the RFCs of each image and provide the estimated accuracy for the RFM fitting solutions, without knowledge of detailed terrain information. It is thus a solution that is terrain-independent. The

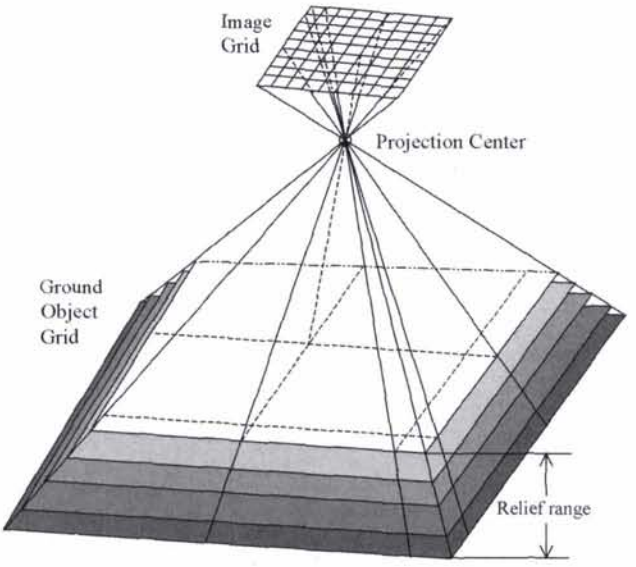

Figure 2. Use of a 3D object grid and image grid to solve the RFM (an illustration for the aerial frame sensor).

solved for RFCs can be provided to users for image ortho-rectification, or for stereo reconstruction if a pair of stereo images each with a set of RFCs is available (Yang, 2000; Tao and Hu, 2001b). This characteristic of the RFM is very attractive because users can make use of the images without knowing the physical sensor model that might be treated as confidential information by commercial vendors. On the other hand, the users do not need to change the ortho-rectification and stereo reconstruction software if the software was developed based on the RFM. The software can also be used to deal with images acquired by different sensors as long as the RFCs of each image are provided.

Terrain-Dependent Computational Scenarios

With no physical sensor models at hand, the 3D object grid cannot be established. Therefore, the GCPs and checkpoints have to be collected in a conventional manner (e.g., from maps or a DEM). In this case, the solution is highly dependent on the actual terrain relief, the number of GCPs, and their distribution across the scene. This method is obviously terrain-dependent. This is a popular approach for image rectification of remote sensing imagery when the rigorous physical sensor model is not available, and when the accuracy requirement is not stringent.

Because the RFM has a very high fitting capability, we are interested in comparing these two computational scenarios in terms of accuracy and numerical stability. The testing results will be discussed in a later section.

Robust Bucketing for Automatic Selection of GCPs

For terrain-dependent scenarios, different results can be obtained with different input control information, such as the number of GCPs and their distribution. Given a set of known control points, the question is how to select a group of control points by which the RFM can reach the best overall fitting accuracy. In other words, how do we select a group of points that are evenly distributed in each dimension? To address this question, we developed a robust bucketing method for automatic selection of GCPs from a given set of control points.

Bucketing Technique

This method is based on a regular random selection bucketing technique (Zhang *et al.*, 1995). The idea of selecting a subset of points that are evenly distributed is not to select more than one point for a given neighborhood. The bucketing technique is given as follows:

First, the minimum and maximum of the planimetric coordinates of the entire point set in the ground space are calculated. Then the test region is divided into $w \times w$ (e.g., $w = 8$) buckets shown in Figure 3 (from Zhang (1995)). Each bucket may contain a number of points, and the buckets having no points are excluded. To generate a subset of n GCPs, we select the two points with maximum and minimum elevation values, then randomly select $n - 2$ mutually different buckets and choose one point in each selected bucket randomly.

However, the number of points in a bucket may be quite different from one to another. There is, consequently, a higher probability of selecting a point pertaining to a bucket having fewer points. In order for each point to have almost the same probability of being selected, it is thus preferred that a bucket having more points should have a higher probability of being selected than a bucket having fewer points. This is to ensure that points selected are evenly distributed. This concept can be realized using the following procedure (Buckley, 1994; Zhang, 1995): if there are in total L buckets, we divide the range [0, 1] into L intervals such that the length of the i^{th} interval is equal to $l_i/\Sigma_i l_i$, where l_i is the number of points attached to the i^{th} bucket shown in Figure 3. During the bucket selection procedure, a random number from [0, 1], generated by a uniform random generator and falling in the i^{th} interval, implies that the i^{th} bucket is selected. Then a point in the i^{th} bucket is randomly selected as a GCP and is excluded from the next selection.

Robust Selection of GCPs

The bucketing technique only accounts for the planimetric distribution of points and not for the vertical (elevation) distribution. In addition, the generated subset is not unique. Because the program executes several times, the produced RFM results may be not comparable. In order to determine the best subset, we could, theoretically, complete trials for all the possible subsets. The best subset is the one in which the RMS (root-mean-square) error of the solution at checkpoints is minimum. For example, given 71 input points, the number of subsets each with 64 points is $C_{71}^{64} \approx 1.33 \times 10^9$. This is computationally impossible in practice, especially when the number of input points is large. Thus, we choose $t(\geq 1)$ trials in such a way that the probability of at least one subset with evenly distributed points will be a large value λ close to 1. Because the entire set has been divided into L buckets, the expression for this probability is

$$\lambda = 1 - (1 - \alpha^{n/L})^t \tag{14}$$

where α is the probability measuring the extent to which the entire set distributes evenly; then $\alpha^{n/L}$ is the probability of obtaining a perfect subset by bucketing. In our experiments, α

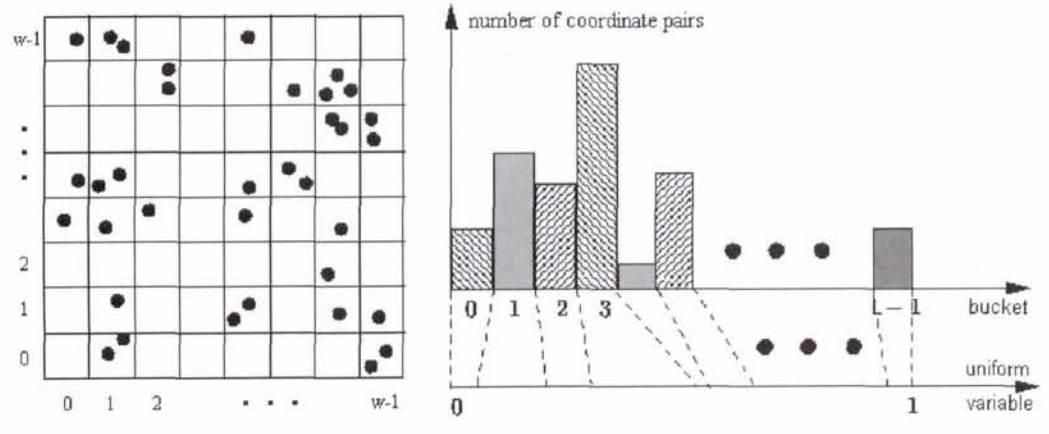

Figure 3. Automatic selection of GCPs based on the bucketing technique.

TABLE 1. NUMBER OF TRIALS (t VS. λ AND α) FOR AUTOMATIC SELECTION OF GCPS

		λ			
	t	.9	.95	.99	.9999
α	99%	1	1	1	2
	95%	1	1	2	4
	90%	1	2	2	5
	80%	2	3	4	7
	60%	5	6	9	17

is defined as $L/(w \times w)$ and is usually a value close to 1. Then t can be computed using

$$t = \left\lceil \frac{\ln(1 - \lambda)}{\ln(1 - \alpha^{n/L})} \right\rceil. \quad (15)$$

This method is a simple variation to the random sample consensus paradigm (Fischler and Bolles, 1981). As shown in Table 1, the number of bucketing trials for given λ and α, when n and w are known (e.g., $n = 64$; $w = 8$), is much less than the possible combinations even if a very high reliability is ensured. For example, when α is 80 percent, only four trials are needed to reach a probability as high as 0.99.

Test Results and Evaluation

Design of Tests

In order to provide a comprehensive evaluation of the RFM, the tests have been designed for these purposes:

- to evaluate the overall fitting accuracy of the RFM under nine different cases, i.e., three different polynomial orders against three different denominator configurations (see Table 2);
- to compare the RFM performance resulting from the two scenarios, terrain-independent scenario versus terrain-dependent;
- to compare the RFM results derived using the direct least-squares solution and the iterative least-squares solution;
- to evaluate the numerical stability of the RFM solutions as well as the effects of regularization method;
- to evaluate the RFM results based on the GCPs selected using the developed automatic method in the case of terrain-dependent scenario; and
- to evaluate the sensitivity of the RFM to the input control information (number and distribution of GCPs).

Table 2 shows the number of unknown RFCs and the required minimum number of GCPs under these nine cases. It is worth noting that the case of $p2 = p4 \equiv 1$ is a regular 3D polynomial model, and the case of $p2 = p4$ with the first order is the Direct Linear Transformation (DLT) model. For the regular 3D polynomial model, only the direct least-squares solution is applied.

TABLE 2. NINE CASES FOR THE RFM TESTS

Order of Polynomials	Cases	Number of RFCs	Min. Number of GCPs
3	$p2 \neq p4$	78	39
	$p2 = p4$	59	30
	$p2 = p4 \equiv 1$	40	20
2	$p2 \neq p4$	38	19
	$p2 = p4$	29	15
	$p2 = p4 \equiv 1$	20	10
1	$p2 \neq p4$	14	7
	$p2 = p4$	11	6
	$p2 = p4 \equiv 1$	8	4

Test Data Sets

Aerial Photograph Data (provided by ERDAS Inc., USA)

The original stereo image pair at a scale of 1:40,000 was taken over Colorado Springs, Colorado, and was scanned at 100 micrometers per pixel. Within the overlap area of the stereo pair, 7499 well distributed points in the left image and their corresponding points in the right image were determined using an automatic image matching algorithm. The ground coordinates of these 7499 points were intersected using the rigorous collinearity equations established after a photogrammetric bundle block adjustment with ERDAS OrthoBASE. The average standard deviations after adjustment in ground space are $(m_X, m_Y, m_Z) = (1.7008, 2.1577, 0.2957)$ meters at five control points, and $(m_X, m_Y, m_Z) = (4.2964, 0.7726, 3.8165)$ meters at one checkpoint. The above processing was done by ERDAS Inc. The left image is used in the experiments. Figure 4 shows a 3D view of the terrain surface generated using these ground points. Other relevant information is given in Table 3.

SPOT Data Set I (provided by ERDAS Inc., USA)

The original image pair is part of the example data in ERDAS IMAGINE OrthoBASE (Yang, 2000). They were taken over the Palm Springs, California region. The relief range is from −75.0 meters to +3414.0 meters. The overlap between the two images is about 60 percent. The image sizes are 6000 by 6000 pixels with 13 micrometers for a pixel, and the ground pixel size is 10 meters. The physical sensor parameters of both images were derived using the OrthoBASE block triangulation software. The unit-weight RMS errors are 0.3 pixels. The grid consists of five layers each with 11 by 11 points. These coordinates were calculated using a rigorous physical sensor model in OrthoBASE by considering Earth curvature. An independent set of 21 by 21 checkpoints on the actual terrain surface was generated based on the inverse form of the corresponding rigorous model of the left image (Yang, 2000). Part of the information is shown in Table 3, and a 3D view of the distribution of the 441 checkpoints is shown in Figure 5.

SPOT Data Set II (provided by PCI Geomatics, Canada)

In total, 71 ground control points and the corresponding image points were collected manually. Figure 6 shows a 3D view of the distribution of these points on the terrain surface. Most of

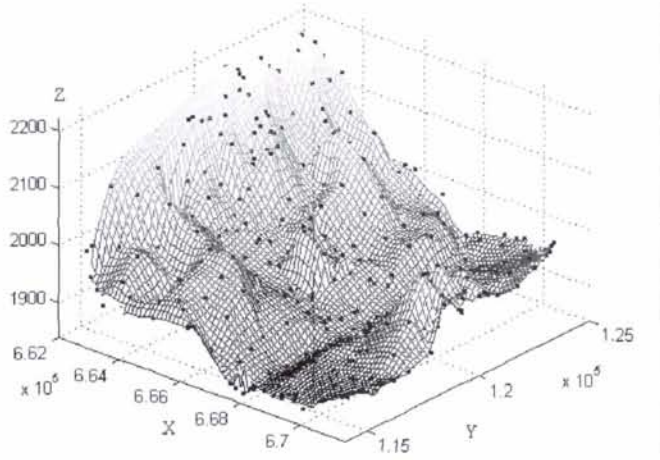

Figure 4. 3D view of the terrain surface from the aerial photograph data.

TABLE 3. INFORMATION ON THE THREE DATA SETS

Data Set	Image Size (pixel)	Ground Pixel Size (meters)	Film Pixel Size (mμ)	Location	Elevation Range (meters)
Aerial Frame	2313 × 2309	4.5	100	Colorado Springs, CO	1846.6 ~ 2205.1
SPOT I	6000 × 6000	10	13	Palm Springs, CA	−75.0 ~ 3414.0
SPOT II	6000 × 6000	10	13	N/A	1.8 ~ 1128.3

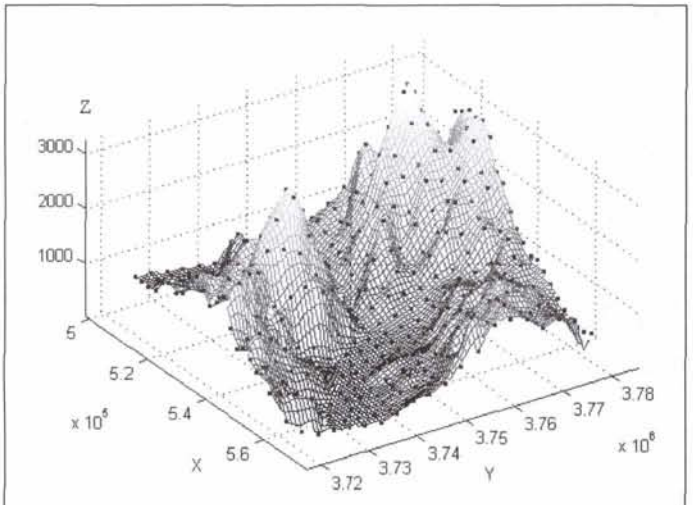

Figure 5. 3D view of the distribution of checkpoints from the SPOT data I.

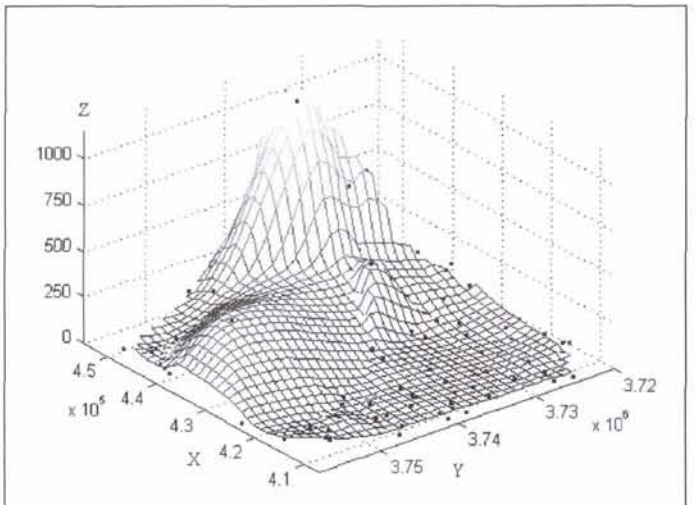

Figure 6. 3D view of the distribution of points from the SPOT data II.

the points are situated on a flat foothill, while only a few appear in the mountain area. Other information is given in Table 3. The accuracy of point measurements is not known.

Experiments and Evaluation : Terrain-Independent Scenario

Accuracy Aspect—Aerial Photograph Data

A rigorous physical sensor model based on the collinearity equations was developed using the imaging parameters provided by ERDAS Inc. An image grid as well as its corresponding control grid and check grid in object space were generated using the rigorous sensor model established. The RFCs were then solved for using the control grid coordinates and the corresponding image coordinates. The accuracy of the solution was examined by comparing the differences in the image coordinates of the check grid computed using the generated RFM and using the rigorous sensor model. Tests under nine different cases (Table 2) were performed. Both the direct and the iterative solutions were also used. A portion of the experimental results using the iterative solution without regularization are given in Table 4. Both the RMS errors and the maximum errors in the image at the control points (CNPs) and the checkpoints (CKPs) are listed. This result is based on the established control grid consisting of five elevation layers each with 10 by 10 grid points, and the check grid consisting of ten elevation layers each with 20 by 20 grid points.

Based on this test, the following findings were obtained:

- The approximating accuracy of the RFM with denominators (*cases* $p2 \neq p4$ and $p2 = p4$) is extremely high and is significantly better than the regular polynomial cases ($p2 = p4 \equiv 1$). The accuracy reaches the level of 10^{-8} to 10^{-13} pixels in comparison to the regular polynomial cases where the accuracy level is at 10^{-1} to 10^{-3} pixels for the second- and third-order polynomials. This shows that the RFM with rational components (denominators) resembles the collinearity equations well and has no accuracy loss for the aerial photograph data.
- The cases of first-order RFM with denominators gain the best results at both CNPs and CKPs (shaded area in Table 4). It indicates that the higher order RFM may not be necessary when dealing with aerial frame data sets.

Accuracy Aspect—SPOT Data I

In this test, the provided 3D object grid was used to solve the RFM, and 441 checkpoints from an actual DEM were used for accuracy checking. The test results obtained using the direct solution without regularization are provided in Table 5. The following findings can be summarized:

- The approximation accuracy is also extremely high for the cases when the second- or the third-order polynomial is used (shaded area in Table 5). The accuracy can reach 10^{-2} at CKPs. The maximum errors are also controlled under 0.06 pixels.
- None of the first-order cases perform well compared to the aerial photography test in which the cases (first-order RFM with denominator) gain the best results (see shaded areas in Table 4).
- The RFM cases with denominator always perform better than the regular polynomials but the third-order regular polynomial model can reach the same level of accuracy at CKPs.
- The RFM cases with unequal denominator ($p2 \neq p4$) perform better than the cases with equal denominator ($p2 = p4$).

Computation Aspect of Terrain-Independent Scenario

In the above two tests, an object grid was used to solve for the RFM. It was found that the condition of the design matrix in normal Equation 11 is always good and regularization of the normal equation is not necessary. The accuracy obtained with the iterative solution is only slightly better than that obtained with the direct solution. Therefore, the direct solution method is recommended due to its simplicity and no requirements for iterations.

TABLE 4. RMS (MAX). ERRORS IN IMAGE WITH THE AERIAL PHOTOGRAPH DATA (UNIT: PIXELS)

Case	First-Order		Second-Order		Third-Order	
	at CNPs	at CKPs	at CNPs	at CKPs	at CNPs	at CKPs
$p2 \neq p4$	3.2999e−13	2.4889e−13	4.1802e−12	4.0645e−12	4.6892e−11	5.7318e−11
	(9.1212e−13)	(1.0268e−12)	(1.7463e−11)	(8.9593e−12)	(1.1330e−09)	(2.4036e−09)
$p2 = p4$	3.2315e−13	3.0909e−13	1.4361e−12	6.2962e−11	8.2839e−10	1.3307e−10
	(1.0240e−12)	(1.3055e−12)	(7.6732e−12)	(5.4024e−09)	(2.0271e−08)	(7.1234e−09)
$p2 = p4 \equiv 1$	1.3245e+01	6.8112e+00	1.7074e−01	1.2095e−01	1.8888e−03	1.6005e−03
	(3.0661e+01)	(2.2807e+01)	(3.5749e−01)	(2.9604e−01)	(4.4959e−03)	(3.5362e−03)

TABLE 5. RMS (MAX.) ERRORS IN IMAGE WITH SPOT DATA I (UNIT: PIXELS)

Case	First-Order		Second-Order		Third-Order	
	at CNPs	at CKPs	at CNPs	at CKPs	at CNPs	at CKPs
$p2 \neq p4$	4.9447e−01	4.4418e−01	9.9060e−04	1.7495e−02	9.9590e−06	1.7662e−02
	(1.4515e+00)	(1.4376e+00)	(3.2228e−03)	(5.3114e−02)	(2.7250e−05)	(5.4008e−02)
$p2 = p4$	9.9014e+00	8.7987e+00	2.7095e−01	2.4712e−01	6.1719e−05	1.7658e−02
	(2.5857e+01)	(2.3307e+01)	(6.7387e−01)	(6.3279e−01)	(2.1711e−04)	(5.3991e−02)
$p2 = p4 \equiv 1$	1.2945e+01	1.1568e+01	4.4997e−01	4.0103e−01	5.1772e−03	1.8122e−02
	(3.0244e+01)	(2.5378e+01)	(1.3680e+00)	(1.2324e+00)	(2.1739e−02)	(5.5622e−02)

The number of layers used in the object grid affects the numerical stability of the RFM. The design matrix becomes singular and the normal equation is ill-conditioned if only two or three elevation layers in the object grid are used. However, the approximation accuracies are very close when four or more layers are used.

Experiments and Evaluation : Terrain-Dependent Scenario

Accuracy Aspect—Aerial Photograph Data

In the terrain-dependent scenario, the GCPs are from the real terrain surface. For a comparison, we used the same data set, aerial photograph data from ERDAS, in which 7499 ground points on the terrain surface are available. In this test, 100 points out of 7499 points were first selected as GCPs using the automatic bucketing selection method, and the remaining points are treated as checkpoints. Due to the good distribution of these points, only one trial was needed in the bucketing selection process. As described earlier, this selection ensures that these 100 GCPs are evenly distributed from the given 7499 points.

In order to provide a reliable assessment on accuracy, the rigorous collinearity equations were used to transform these 7499 points to both the left and right images. The obtained accuracy of the RFM solution based on the 100 GCPs and the 7399 checkpoints, as well as their corresponding image points, is shown in Table 6. The results are computed from the left image using the direct least-squares solution with regularization ($h = 0.001$).

- This result shows that, under the terrain-dependent scenario, the RFM can also achieve a high approximation accuracy (i.e., RMS <5.0e − 02 at CKPs), if the control points are adequate and evenly distributed for the aerial frame data. However, the level of approximation is not as high as that in the terrain-independent scenario.
- The RFM cases with denominator are better than the regular polynomial models overall, but the accuracy of the third-order regular polynomial model is still very good.
- It is interesting that, from Table 6, the case $p2 \neq p4$ always has a better fitting accuracy than the case $p2 = p4$ at CNPs for different orders, but the case $p2 = p4$ works better than the case $p2 \neq p4$ at CKPs. However, there is no significant difference between both cases.
- The first-order RFM cases (shaded areas in Table 6) gain higher accuracy at CKPs, while the third-order RFM cases have higher accuracy at CNPs. None of these cases can achieve the best accuracy at both CNPs and CKPs. This implies that the RFM approximation has not achieved the best numerical status under the terrain-dependent scenario. Therefore, for terrain-dependent solutions, one may need to try different orders in order to determine the best RFM case or the best trade-off.

Computation Aspect—Aerial Photograph Data

- Due to the fact that the design matrix is almost rank-deficient under the terrain-dependent scenario, regularization is particularly important especially for the cases with the second- and third-order polynomials. Table 7 shows a comparison of results solved for with and without the use of regularization (Table 6 is the result with regularization). The improvements are very significant in terms of accuracy. It is worth mentioning that regularization also makes the solutions converge. This result indicates that the numerical stability of the RFM may be poor under the terrain-dependent scenario, although it is able to

TABLE 6. RMS (MAX.) ERRORS IN IMAGE WITH FRAME DEM DATA (TERRAIN-DEPENDENT SCENARIO, UNIT: PIXELS)

Case	First-Order		Second-Order		Third-Order	
	at CNPs	at CKPs	at CNPs	at CKPs	At CNPs	At CKPs
$p2 \neq p4$	4.2924e−02	4.8997e−02	3.9456e−02	5.1097e−02	3.4249e−02	6.1061e−02
	(1.4295e−01)	(1.8368e−01)	(1.3810e−01)	(2.2157e−01)	(9.8376e−02)	(4.1028e−01)
$p2 = p4$	4.3337e−02	4.8632e−02	4.0481e−02	5.0317e−02	3.5615e−02	5.5134e−02
	(1.3760e−01)	(1.6649e−01)	(1.3900e−01)	(2.0361e−01)	(1.0335e−01)	(2.8847e−01)
$p2 = p4 \equiv 1$	3.9114e+00	4.7346e+00	4.7345e−02	6.7922e−02	3.7685e−02	5.5159e−02
	(1.0164e+01)	(2.6154e+01)	(1.4400e−01)	(5.5222e−01)	(1.0750e−01)	(2.9220e−01)

TABLE 7. EFFECTS OF REGULARIZATION FOR ACCURACY IMPROVEMENTS (UNIT: PIXELS)

Case	Order	Regularization	RMS at CNPs	Max at CNPs	RMS at CKPs	Max at CKPs
	1	h = 0	4.2924e−02	1.4294e−01	4.9006e−02	1.8375e−01
		h = 0.001	4.2924e−02	1.4295e−01	4.8997e−02	1.8368e−01
$p2 \neq p4$	2	h = 0	9.2097e−02	5.5913e−01	1.5101e+00	7.5617e+01
		h = 0.001	3.9456e−02	1.3810e−01	5.1097e−02	2.2157e−01
	3	h = 0	7.0171e−02	2.5211e−01	6.3360e+00	5.3717e+02
		h = 0.001	3.4249e−02	9.8376e−02	6.1061e−02	4.1028e−01
	1	h = 0	4.3339e−02	1.3759e−01	4.8654e−02	1.6661e−01
		h = 0.001	4.3340e−02	1.3756e−01	4.8646e−02	1.6657e−01
$p2 = p4$	2	h = 0	7.2629e−02	3.3755e−01	2.5887e+00	1.8341e+02
		h = 0.001	4.0481e−02	1.3900e−01	5.0317e−02	2.0361e−01
	3	h = 0	8.2221e−02	4.4792e−01	3.1974e+00	2.4258e+02
		h = 0.001	3.5615e−02	1.0335e−01	5.5134e−02	2.8847e−01

achieve a high approximation accuracy provided the GCPs are adequate and well distributed.

- For this data set, due to the adequate number of well-distributed GCPs, the accuracy obtained by the direct solution is comparable to that from the iterative solution. Therefore, only the results from the direct solution are given in Table 7.
- Figure 7 shows the relationship between the number of GCPs used (from 40 to 1600) and the accuracy obtained at CKPs. In Figure 7, the computation result is based on the third-order RFM with unequal denominator case where the required minimum number of GCPs is 39 (see Table 2). It can be observed from Figure 7 that the accuracy will not be improved much once the number of GCPs used is larger than 80 (which doubles the required minimum number, 39). This is a useful finding because the use of too many GCPs would not be beneficial to the accuracy. It also indicates that the proposed automatic selection method of GCPs is efficient.

Accuracy Aspect—SPOT Data II

Sixty-four out of the total given 71 GCPs were selected automatically using the robust bucketing method, and the remaining points were used as checkpoints. It is a fact that the distribution of these GCPs (see Figure 5) is not good. The obtained a is only 56.3 percent (see Equation 14) and the number of trials is seven when the probability λ is assumed to be 95 percent. The results shown in Table 8 were computed using the iterative least-squares method with regularization ($h = 0.001$). The following findings were obtained:

- Because the available GCPs are not evenly distributed, the obtained accuracy is only at the one-pixel level. This is understandable because the RFM solution is sensitive to the distribution of GCPs under the terrain-dependent scenario.

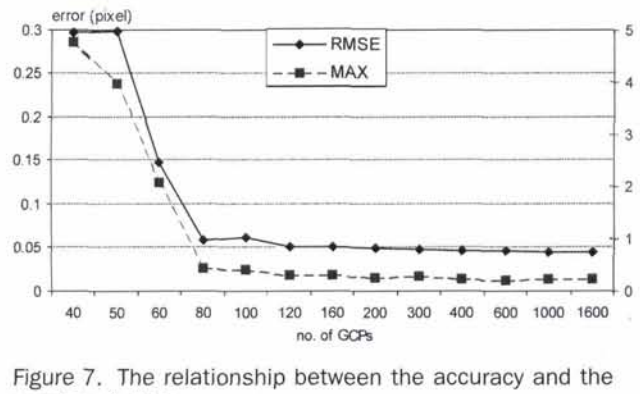

Figure 7. The relationship between the accuracy and the number of GCPs.

- The third-order case $p2 \neq p4$ gains the best approximation accuracy at the CKPs, while the regular 3D polynomial model reaches the same level of accuracy at the CKPs.
- The cases with denominator are better than the regular polynomial cases ($p2 = p4 \equiv 1$).
- The cases with non-equal denominator ($p2 \neq p4$) are always better than the cases with equal denominator ($p2 = p4$). This conclusion is the same as that from the SPOT data I test under the terrain-independent scenario.
- For this data set, the higher the order, the better the approximation accuracy.

Computation Aspect—SPOT Data II

The iterative least-squares solution with regularization provides better results than does the direct solution. This result shows that the iterative solution with regularization is much more robust. It performs best for data sets in which the normal equations are not well-conditioned or GCPs are not well distributed. More comparative experiments have been reported in Tao and Hu (2000a; 2000b).

Conclusions and Discussions

In this paper, the iterative and direct least-squares solutions to the RFM are derived. The regularization technique is proposed to improve the solutions when the condition of the normal equations is poor. The terrain-independent and terrain-dependent scenarios are analyzed and compared. Based on the numerous tests, the following conclusions can be drawn:

With the physical sensor model available—terrain-independent scenario:

- The RFM can approximate the rigorous physical sensor model extremely well for aerial frame data and SPOT pushbroom data used in the tests. Thus, it can be used as a replacement sensor model to communicate to end users for photogrammetric processing such as ortho-rectification and stereo reconstruction.
- The high order RFM may not be necessary when dealing with aerial frame data sets, because the RFM resembles the projective model very well. However, the high order RFM is preferable when SPOT data are processed.
- The RFM cases with unequal denominator achieve a better accuracy than the cases with equal denominator at CKPs overall. The RFM cases with denominator perform better than the regular polynomials, but the regular third-order polynomial model can achieve an accuracy that is also reasonably good.
- The conditions of normal equations are very good. The iterative least-squares solution is only slightly better than the direct least-squares solution. There is no need to apply regularization. The direct solution without regularization is recommended for solving the RFM due to its simplicity and no iterations involved.
- In the establishment of the 3D object grid for the RFM solutions, at least four or more elevation layers are needed, otherwise, the design matrix would be singular.

TABLE 8. RMS (MAX.) ERRORS IN IMAGE WITH SPOT DATA II (TERRAIN-DEPENDENT SCENARIO, UNIT: PIXELS)

Case	First-order		Second-order		Third-order	
	at CNPs	at CKPs	at CNPs	at CKPs	at CNPs	At CKPs
$p2 \neq p4$	8.1319e−01	1.6951e+00	7.1123e−01	1.5444e+00	3.9926e−01	1.4446e+00
	(1.9953e+00)	(2.5683e+00)	(1.5059e+00)	(2.3522e+00)	(1.0145e+00)	(2.3238e+00)
$p2 = p4$	3.0468e+00	9.4872e+00	8.1556e−01	2.2067e+00	5.8962e−01	2.1393e+00
	(7.8451e+00)	(1.8124e+01)	(1.7738e+00)	(3.5475e+00)	(1.2006e+00)	(3.0912e+00)
$p2 = p4 \equiv 1$	3.7589e+00	1.2530e+01	7.7128e−01	1.6104e+00	6.4575e−01	1.6533e+00
	(1.1063e+01)	(2.4935e+01)	(1.9939e+00)	(2.3341e+00)	(1.4080e+00)	(2.5031e+00)

With the physical sensor model unknown—*terrain-dependent scenario*:

- The RFM can also achieve a good approximation accuracy provided the GCPs are adequate and are evenly distributed. However, the accuracy of the approximation is not as high as that in the terrain-independent scenario. Moreover, in practice, it is not easy to collect an "adequate number" of GCPs.
- The RFM solution is sensitive to the distribution of GCPs as well as to the number of GCPs. The result cannot be expected to be good once the distribution of the GCPs is not good (see tests on SPOT Data II).
- It is difficult to determine which case of the RFM can provide the best result, because the solution is not numerically stable. Therefore, one may need to try different cases to determine the best RFM case (i.e., order) or to find the best trade-off.
- The design matrix is almost rank-deficient; therefore, regularization is extremely important, especially for the high order RFM cases. Use of regularization to improve the conditions of the design matrix will result in a much better accuracy and make the solutions converged.
- The iterative least-squares solution always offers better results than does the direct solution, particularly for the terrain-dependent scenario. Therefore, the iterative least-squares method with regularization should be adopted for solving the RFM under the terrain-dependent scenario.
- The proposed method on automatic selection of GCPs is useful for improving the numerical stability of RFM solutions because the method can produce from the given control points a set of GCPs that are evenly distributed.

Consequently, the RFM determined under the terrain-independent scenario can offer a robust and very accurate approximation to the rigorous physical sensor model. The RFM solutions derived from the terrain-dependent scenario are sensitive to the number of GCPs and their distribution, and are not numerically stable. Based on the concept that the RFM can be used to deal with different sensor imagery, a prototype system, Rational Mapper, has been developed for the RFM-based orthorectification and stereo reconstruction using images whose RFCs are provided (Tao and Hu, 2001a; Tao and Hu, 2001b). The advantage of the system is that the software is sensor independent and the photogrammetric processing becomes versatile.

It is a fact that the RFM solutions are usually determined by the data vendor using a proprietary physical sensor model. The accuracy of the RFM solutions is dependent on the availability and the usage of the GCPs (Grodecki, 2001). If accurate RFM solutions are required, GCPs are needed and are incorporated into the RFM solution process. In many cases, GCPs are not available at the time of processing or cannot be supplied due to some reasons (e.g., politics or confidentiality). Hu and Tao (2001) have investigated a method to update and improve the existing RFM solutions (provided, for example, by the vendor) with additional GCPs using the Kalman-filter-based incremental technique and covariance propagation.

Because low-order RFM cases may obtain better approximating accuracy, a remaining problem with the high-order RFM cases is their over-parameterization because of an excessive number of coefficients. This causes instability in the least-squares solution. Madani (1999) proposed selecting the significant coefficients for a particular sensor by the trial-and-error method. In this paper we used the regularization technique with some success to overcome this drawback. Further investigations on the accuracy analysis of high resolution images (such as IKONOS-2 imagery) using the RFM approach are of interest (Tao and Hu, 2001b).

Acknowledgments

Discussions with Drs. Xinghe Yang and Yongnia Wang from ERDAS Inc., Dr. Philip Cheng from PCI Geomatics, Dr. Thierry Toutin from the Canada Centre for Remote Sensing, Mr. Brian Robertson from MacDonald Dettwiler and Associates Ltd., Dr. Clive Fraser from the University of Melbourne, and Prof. Gordon Petrie from the University of Glasgow were extremely valuable. We also appreciate the comments made by Dr. Mostafa Madani from Z/I Imaging, Dr. Ian Dowman from University College London, Mr. Kris Morin from LH systems, as well as anonymous reviewers. Special thanks go to ERDAS Inc. (Drs. X. Yang and Y. Wang), PCI Geomatics (Dr. P. Cheng), and Intermap Technologies (Dr. J. Bryan Mercer) for providing test data sets to support the research.

References

Buckley, J.J., 1994. Fuzzy genetic algorithm and applications, *Fuzzy Sets and Systems*, 61(2):129–136.

Burden, R.L., and J.D. Faires, 1997. *Numerical Analysis, Sixth Edition*, Brooks/Cole Publishing Company, Pacific Grove, California, 811 p.

Dowman, I., and J.T. Dolloff, 2000. An evaluation of rational functions for photogrammetric restitution, *Int'l Achieve of Photogrammetry and Remote Sensing*, 33(Part B3):254–266.

Fischler M.A., and R.C. Bolles, 1981. Random sample consensus: A paradigm for model fitting with applications to image analysis and automated cartography, *Communications of the ACM*, 24(6):381–395.

Greve, C.W., C.W. Molander, and D.K. Gordon, 1992. Image processing on open systems, *Photogrammetric Engineering & Remote Sensing*, 58(1):85–89.

Grodecki, J., 2001. IKONOS stereo feature extraction—RPC approach. *Proceedings of 2001 ASPRS Annual Convention* (CD ROM), 23–27 April, St. Louis, Missouri, unpaginated.

Hu, Y., and C.V. Tao, 2001. Updating solutions of the rational function model using additional control points for enhanced photogrammetric processing, *Proceedings of Joint ISPRS Workshop on "High Resolution Mapping from Space 2001"* (CD ROM), 19–21 September, Hannover, Germany, unpaginated.

Madani, M., 1999. Real-time sensor-independent positioning by rational functions. *Proceedings of ISPRS Workshop on "Direct versus Indirect Methods of Sensor Orientation"*, 25–26 November, Barcelona, Spain, pp. 64–75.

McGlone, C., 1996. Sensor modeling in image registration, *Digital Photogrammetry: An Addendum* (C. W. Greve, editor), American Society for Photogrammetry and Remote Sensing, Bethesda, Maryland, pp. 115–123.

Neumaier, A., 1998. Solving ill-conditioned and singular linear system, *SIAM Review*, 40(3):636–666.

NIMA (National Imaging and Mapping Agency), 2000. *The Compendium of Controlled Extensions (CE) for the National Imagery Transmission Format (NITF), Version 2.1*, URL: http://www.ismc.nima.mil/ntb/superceded/STDI-0002_v2.1.pdf

OGC (OpenGIS Consortium), 1999. *The OpenGIS Abstract Specification—Topic 7: The Earth Imagery Case*, URL: http://www.opengis.org/public/abstract/99–107.pdf.

Paderes, Jr, F.C., E.M. Mikhail, and J.A. Fagerman, 1989. Batch and on-line evaluation of stereo SPOT imagery, *Proceedings of the ASPRS-ACSM Convention*, 02–07 April, Baltimore, Maryland, pp. 31–40.

Tao, C.V., and Y. Hu, 2000a. Investigation on the Rational Function Model, *Proceedings of 2000 ASPRS Annual Convention* (CD ROM), 24–26 May, Washington, D.C., unpaginated.

———, 2000b. Study of the rational function model for image rectification, *Proceedings of Canadian Conference on Remote Sensing*, 22–25 August, Victoria, BC, Canada, pp. 55–64.

———, 2001a. The rational function model: A tool for processing high-resolution imagery, *Earth Observation Magazine* (EOM), 10(1):13–16.

———, 2001b. 3-D reconstruction algorithms with the rational function model and their applications for IKONOS stereo imagery, *Proceedings of Joint ISPRS Workshop on "High Resolution Mapping from Space 2001"* (CD ROM), 19–21 September, Hannover, Germany, unpaginated.

Toutin, T., and P. Cheng, 2000. Demystification of IKONOS, *Earth Observation Magazine* (EOM), 9(7):17–21.

Yang, X., 2000. Accuracy of rational function approximation in photogrammetry, *Proceedings of 2000 ASPRS Annual Convention* (CD ROM), 22–26 May, Washington D.C., unpaginated.

Zhang, Z., R. Deriche, O. Faugeras, and Q.T. Luong, 1995. A robust technique for matching two uncalibrated images through the recovery of the unknown epipolar geometry, *Artificial Intelligence*, 78(1–2):87–119.

(Received 07 February 2001; accepted 10 May 2001; revised 17 August 2001)